NANO LETTERS

pubs.acs.org/NanoLett Letter

Topological Nodal-Point Superconductivity in Two-Dimensional Ferroelectric Hybrid Perovskites

Xiaoyin Li, Shunhong Zhang, Xiaoming Zhang, Zeev Valy Vardeny, and Feng Liu*

Cite This: *Nano Lett.* 2024, 24, 2705−2711 Read Online

ACCESS | Metrics & More | Article Recommendations | Supporting Information

ABSTRACT: Two-dimensional (2D) hybrid organic−inorganic perovskites (HOIPs) with enhanced stability, high tunability, and strong spin−orbit coupling have shown great potential in vast applications. Here, we extend the already rich functionality of 2D HOIPs to a new territory, realizing topological superconductivity and Majorana modes for fault-tolerant quantum computation. Especially, we predict that room-temperature ferroelectric BA_2PbCl_4 (BA for benzylammonium) exhibits topological nodal-point superconductivity (NSC) and gapless Majorana modes on selected edges and ferroelectric domain walls when proximity-coupled to an s-wave superconductor and an in-plane Zeeman field, attractive for experimental verification and application. Since NSC is protected by spatial symmetry of 2D HOIPs, we envision more exotic topological superconducting states to be found in this class of materials due to their diverse noncentrosymmetric space groups, which may open a new avenue in the fields of HOIPs and topological superconductivity.

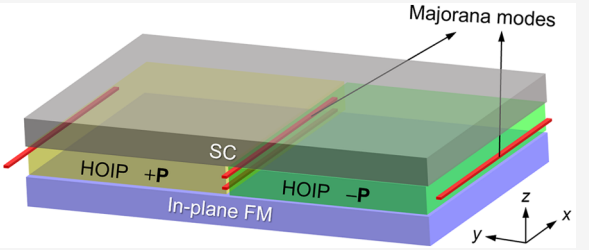

KEYWORDS: *two-dimensional, ferroelectric hybrid perovskites, topological nodal-point superconductivity, edge/domain-wall Majorana modes*

Downloaded via UNIV OF UTAH on December 2, 2024 at 23:51:02 (UTC).
See https://pubs.acs.org/sharingguidelines for options on how to legitimately share published articles.

Two-dimensional (2D) hybrid organic−inorganic perovskites (HOIPs) refer to a large family of layered materials that consists of inorganic slabs interleaved with the large organic cation slab as a spacer.[1] The introduction of organic slabs not only enhances the environmental stability but also imposes strong confinement on the inorganic layers, making them natural multiple quantum wells.[2,3] Upon changing the organic cations and/or varying the thickness of the interleaved inorganic slab, 2D HOIPs exhibit impressive structural diversity, as well as tunable physical and chemical properties. Together with the strong spin−orbit coupling (SOC) induced by the heavy metal cations, 2D HOIPs show great promise for photovoltaic, optoelectronic, ferroelectric, and spintronic applications.[4−16] Moreover, due to weak van der Waals (vdW) interactions of the organic spacers, molecularly thin perovskite nanosheets or even perovskite monolayers can be isolated from their bulk crystals by mechanical exfoliation, similar as in vdW 2D materials.[17] The resultant molecularly thin perovskite materials and their heterostructures with other materials are expected to show exotic properties and potentials for widespread applications.[18]

Topological superconductors hosting Majorana boundary modes are long-sought platforms to realize non-Abelian statistics and fault-tolerance quantum computation.[19−23] Intrinsic topological superconductivity (TSC) is rarely present in naturally existing materials, while extrinsic TSC can be realized by utilizing the spin-momentum-locking property of materials,[24] especially the abundant noncentrosymmetric semiconductors.[25] A heterostructure that consists of the semiconductor thin film (or nanowire) sandwiched between a conventional s-wave superconductor (SC) and a ferromagnet (FM) constitutes the simplest platform for realizing TSC[26−28] via effective *p*-wave pairing.[29] Since the first theoretical demonstration of this proposal by employing the Rashba semiconductor InAs,[26] researchers have generalized this extrinsic TSC theory to more generic forms of antisymmetric SOC, including Rashba SOC, Dresselhaus SOC, Weyl SOC, and their linear combinations.[30,31] However, despite extensive experimental efforts, unambiguous evidence of Majorana zero modes in such structures is still lacking.[32] Possible challenges lie in the experimental synthesis of noncentrosymmetric semiconductors with the desired thickness and crystal orientation and fabrication of heterostructures with high-quality interfaces, as well as sizable nontrivial superconducting gap for observing the Majorana modes.[33−35] New candidate materials to circumvent these challenges are highly pursued, especially the essential component of noncentrosymmetric semiconductors.

Here, we propose that the noncentrosymmetric 2D HOIPs can be exploited to achieve nontrivial superconductivity and

Received: October 23, 2023
Revised: January 14, 2024
Accepted: January 16, 2024
Published: January 19, 2024

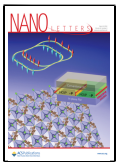

ACS Publications © 2024 American Chemical Society

https://doi.org/10.1021/acs.nanolett.3c04085
Nano Lett. 2024, 24, 2705−2711

gapless Majorana modes. Their 2D vdW nature eases the synthesis of HOIP thin films with intact smooth surfaces and absent dangling bonds, which may also ensure a good quality of interfaces when forming heterostructures and facilitate corresponding device fabrications. Meanwhile, the large SOC-related electronic band splitting of 2D HOIPs is also beneficial for experimental observation of Majorana modes. Specifically, we focus here on 2D HOIP BA_2PbCl_4 ($BA = C_6H_5CH_2NH_3^+$) that has been experimentally demonstrated to possess room-temperature ferroelectricity having the noncentrosymmetric space group $Cmc2_1$ (the point group symmetry is C_{2v}) below the ferroelectric phase transition temperature (~438 K).[36−39] This point group symmetry enables an anisotropic SOC effect, leading to spin splitting or degenerate electronic bands along different crystallographic directions.[13] Using the BA_2PbCl_4 monolayer, in proximity to an *s*-wave superconducting pairing and an in-plane Zeeman field, we demonstrate the emergence of an exotic topological nodal-point superconductivity (NSC) and gapless Majorana edge/domain-wall modes with crystallographic anisotropy, different from the previously reported extrinsic TSC independent of crystallographic orientations.

NSC featuring topologically protected nodal-points in its bulk SC quasiparticle bands has been shown to realize gapless Majorana modes on selected boundaries and studied mainly in material platforms that involve unconventional SC pairings,[40,41] nontrivial normal electronic states,[42−44] or complex magnetic configurations.[45] Recently, its existence has been intensively explored in layered superconducting transition-metal dichalcogenides with interorbital SC pairing,[46,47] and corresponding experimental observations were reported in a novel 4Hb phase of TaS_2.[48] However, its realization by utilizing the spin-momentum-locking property of abundant semiconductors has not yet been investigated so far until the present work. Our study provides a simpler promising material platform to realize NSC by further generalizing SOC forms of semiconductors and sheds light on finding more exotic topological superconducting states by similar schemes. Moreover, given the ferroelectricity of BA_2PbCl_4, its electric polarization as well as the chirality of anisotropic SOC can be switched by an external electric field, realizing ferroelectric NSC as a special candidate of ferroelectric TSC we proposed recently,[49] which renders highly tunable gapless Majorana modes at the inner ferroelectric domain walls.

Figure 1 illustrates TSC and NSC based on noncentrosymmetric semiconductors with the well-studied isotropic Rashba SOC[50] compared to the anisotropic SOC studied here. For Rashba SOC interaction written as $\lambda_R\ (k_x\sigma_y - k_y\sigma_x)$ and exhibiting only in-plane spin textures, the spin degeneracy of the continuum bands is lifted along all crystallographic directions except at the time-reversal-invariant momenta (the Kramers degeneracy) as shown in Figure 1a. An out-of-plane Zeeman field induced by the proximity to an FM would further lift the Kramers degeneracy. After including superconducting pairing, one obtains quasiparticle bands by solving the Bogoliubov−de-Gennes (BdG) Hamiltonian of the Nambu representation to describe the SC excitation states. Given the isotropic Rashba SOC splitting, by tuning the chemical potential and Zeeman energy, *s*-wave pairing can open gaps at all quasiparticle-band-crossing points near the Fermi energy as indicated in Figure 1b that results in TSC with gapless Majorana modes on all edges (Figure 1c). In contrast, for the anisotropic SOC in BA_2PbCl_4, the C_{2v} point group enforces spin-degenerate bands along the *x* direction but splits the spin

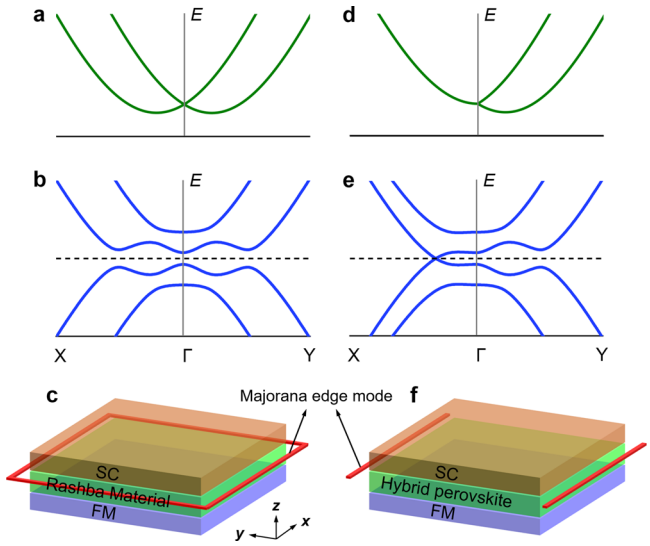

Figure 1. Schematics of TSC vs NSC based on noncentrosymmetric semiconductors with isotropic vs anisotropic SOC. Isotropic SOC: (a) SOC-related split electronic band structure; (b) BdG quasiparticle band structure; (c) Majorana edge mode. Anisotropic SOC: (d−f) same as in (a−c) but for the 2D HOIP with anisotropic SOC. Note the band crossing along the Γ−X direction in (e).

bands along all other directions as shown in Figure 1d. Such an anisotropic SOC effect can be described by an effective $\boldsymbol{k}\cdot\boldsymbol{p}$ Hamiltonian expanded around the Γ point, written as $H_{SOC} = \lambda k_y\sigma_z$ (see Note 1 and Figure S1 in the Supporting Information (SI)), in which the spin textures of the split bands are along the out-of-plane directions. By proximity-coupling to an FM with in-plane magnetization and tuning the chemical potential to appropriate values, *s*-wave pairing can open gaps at the quasiparticle-band-crossing points where the SOC splitting is nonvanishing. But along the Γ−X direction where the SOC splitting is absent and spin is conserved, the quasiparticle-band-crossing point cannot be gapped by conventional *s*-wave pairing. Consequently, the resulting quasiparticle band structure shows spatial-symmetry-protected nodal points along the Γ−X path (Figure 1e) and gapless Majorana modes on the edges terminated along the *y*-direction (Figure 1f). The crystallographic anisotropy of gapless Majorana edge modes follows the same rule as the gapless topological states in Weyl semimetals of the normal state. In the following, we demonstrate the emergence of NSC and anisotropic Majorana edge modes in the BA_2PbCl_4 monolayer based on first-principles calculations (see the SI for the calculation methods).

The optimized atomic structure of the BA_2PbCl_4 monolayer subject to a ferroelectric ground state is shown in Figure 2a, which is the thinnest film of BA_2PbCl_4. It contains two layers of organic cations $[C_6H_5CH_2NH_3]^+$ and a sandwiched inorganic layer of $[PbCl_4]^{2-}$ octahedra connected in a corner-sharing fashion. The arrangement of organic cations results in an *x*-direction ferroelectric polarization, and the direction can be flipped by an external electric field. Although the dimensionality of the BA_2PbCl_4 monolayer is reduced to 2D, its point group remains C_{2v}; therefore, the same SOC form is expected. Figure 2b displays the calculated electronic band structure of the BA_2PbCl_4 monolayer, showing that it is a semiconductor with the conduction band exhibiting large anisotropic spin splitting. The valence band also shows spin splitting, but with a much smaller magnitude. This difference is

https://doi.org/10.1021/acs.nanolett.3c04085
Nano Lett. 2024, 24, 2705−2711

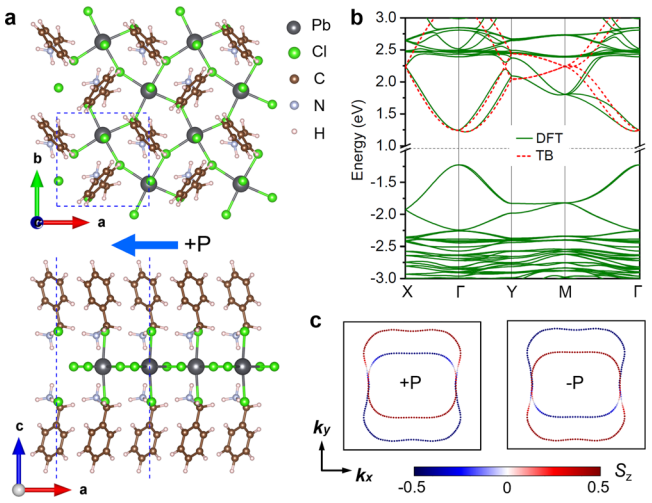

Figure 2. Atomic and electronic structure of the ferroelectric BA_2PbCl_4 monolayer. (a) Top and side views of the atomic structure. The blue arrow (+**P**) indicates the direction of ferroelectric polarization. (b) Electronic band structure along high-symmetry k paths of the Brillouin zone. (c) Conduction band energy contours (E = 1.58 eV) of the BA_2PbCl_4 monolayer with opposite polarization direction (+**P** and −**P**). The S_z component of spin is mapped by the color bar, while the S_x and S_y components are constrained to zero by crystal symmetry.

rooted in their different orbital contributions (Figure S2). For a better property, we focus on the conduction band with large SOC splitting. By calculating the spin textures of split conduction bands, we find that only the S_z component is nonzero while the S_x and S_y components are exactly zero constrained by the crystal symmetry (Figure S3). Figure 2c shows the conduction band energy contours of the BA_2PbCl_4 monolayer with opposite electric polarizations. This figure conveys two key messages: one is the anisotropic band splitting, with perfect degeneracy along the Γ−X direction and giant splitting along all other directions; the other is the interlocking of electric polarization and band spin polarization, which enables switching the chirality of the anisotropic SOC by flipping the electric polarization. These calculation results are consistent with the theoretical analysis of the anisotropic SOC described above and can be well described by the effective Hamiltonian H_{SOC}.

To reveal the physics of the BA_2PbCl_4 monolayer sandwiched by SC and FM layers, we first construct an effective tight-binding (TB) Hamiltonian to describe the conduction band. Using a single orbital per Pb site as the basis (Figure S2), the TB Hamiltonian is written as

$$H_{TB} = \varepsilon \sum_i c_i^\dagger c_i + t \sum_{\langle ij \rangle} c_i^\dagger c_j + i\lambda \sum_{\langle ij \rangle} c_i^\dagger (\hat{\boldsymbol{d}}_{ij,y}\sigma_z) c_j + \sum_i c_i^\dagger (\boldsymbol{B}\cdot\boldsymbol{\sigma}) c_i \quad (1)$$

The first and second terms are the onsite energy and nearest-neighbor hopping, respectively. The third term represents the anisotropic SOC effect of H_{SOC} in the real-space lattice model. Here $\hat{\boldsymbol{d}}_{ij,y}$ is the y-component of the unit nearest-neighbor bond vector $\boldsymbol{d}_{ij}$, and the magnitude and sign of the constant λ encode the strength and direction of the built-in electric field which stems from the ferroelectric polarization induced by structural inversion-symmetry breaking. Switching the ferroelectric polarization flips the direction of the built-in electric field, which is reflected in the model as the sign reversal of λ. The last term accounts for the Zeeman splitting induced by the FM-proximity effect. By fitting the first-principles calculation results of the +**P** polarized BA_2PbCl_4 monolayer, we obtain the parameters of ε = 2.24, t = −0.25, and λ = 0.07 eV, with which the TB Hamiltonian can reproduce well the band-edge physics of the conduction band (Figure 2b). For the −**P** polarized counterpart, λ = −0.07 eV. Including s-wave superconducting pairing, the following BdG Hamiltonian is adopted to describe the SC quasiparticle physics

$$H_{BdG} = \begin{pmatrix} H - \mu & \Delta \\ \Delta^\dagger & -H^* + \mu \end{pmatrix} \quad (2)$$

Here Δ is the s-wave pairing gap induced by SC-proximity effect, and μ represents the chemical potential. H is eq 1 expressed in reciprocal space. Below, we set Δ = 0.05 eV and assume that the proximate FM induces an in-plane Zeeman field along the y-direction. In principle, one needs a Zeeman field that is perpendicular to the spin textures of the SOC-split bands; hence, any in-plane Zeeman field will work for the BA_2PbCl_4 monolayer due to its pure out-of-plane spin-polarization of SOC-split bands. By tuning the chemical potential and Zeeman field to be μ = 1.23 and B_y = 0.1 eV, we solved the BdG Hamiltonian and obtained the quasiparticle band structure. As shown in Figure 3a, a pair of nodal points exist along the Γ−X direction. We calculate the Berry phase (see the SI for calculation details) and obtain the results of $+\pi$ and $-\pi$, or topological charge +1 and −1, respectively, for the left and right nodal points, demonstrating their nontrivial topology to be the same as the Weyl points in 2D.[51,52] The

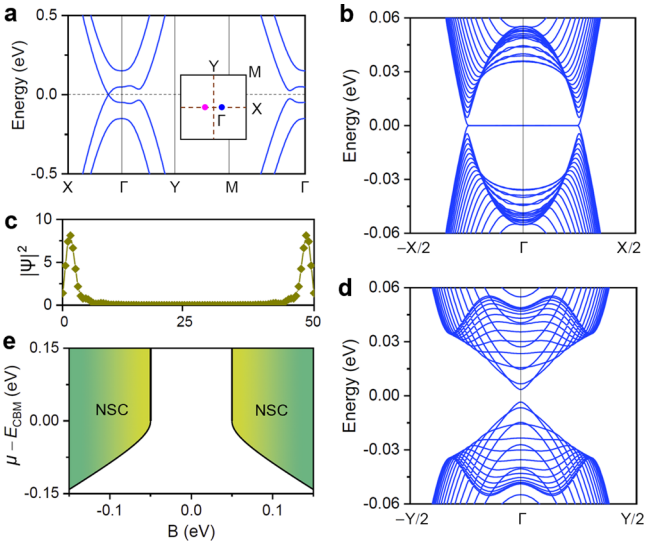

Figure 3. NSC in the BA_2PbCl_4 monolayer. (a) BdG quasiparticle band structure along high-symmetry k paths. Inset plots two nodal points in the Brillouin zone, whose chirality is shown by different colors (purple/blue for ±). (b) and (c) BdG band structure of a nanoribbon terminated along y-direction and real-space distributions of emerged gapless Majorana modes. (d) BdG band structure of a nanoribbon terminated along the x-direction. (e) NSC phase diagram in the parameter space of chemical potential μ and Zeeman field B with a fixed Δ = 0.05 eV. For (a−d), μ = 1.23 and B = 0.1 eV. The widths of the two nanoribbons are both 50 unit cells.

https://doi.org/10.1021/acs.nanolett.3c04085
Nano Lett. 2024, 24, 2705−2711

opposite sign corresponds to the opposite chirality of the two nodal points.

One hallmark of topological superconducting states is the emergence of gapless Majorana modes, which can be verified by constructing a 1D finite system and solving the corresponding BdG Hamiltonian. Figure 3b shows the BdG band structure of a SC/BA_2PbCl_4/FM nanoribbon terminated along the *y*-direction, where one can clearly see the emergence of two gapless Majorana modes. Their real-space distributions indicate that the gapless Majorana modes are localized at the two edges (Figure 3c). We note that here the maximum amplitude of the real-space distribution is in the vicinity of the edges but not exactly at the outmost atomic row, which could be attributed to the chemical environment of the edges. Although topological edge states remain existing as long as their protecting symmetry is preserved, their distributions in both momentum and real spaces are material- and edge-specific and tunable by modifying the chemical potential (environment) of edges.[53,54] We also consider a nanoribbon terminated along the *x*-direction but yield a gapped BdG band structure and the absence of gapless Majorana modes (Figure 3d). These results demonstrate that the emergence of Majorana edge modes has a clear dependence on the crystallographic direction, which can be explained as follows. For the *y*-terminated nanoribbon, the reduced 1D Brillouin zone is periodic along the Γ−X direction. The two nodal points of Figure 3a are still located at different momenta in this reduced Brillouin zone and connected by gapless Majorana modes. While for the *x*-terminated nanoribbon, its 1D Brillouin zone is periodic along the Γ−Y direction. In this case, the two nodal points with opposite chirality are folded into the same momentum and annihilate, resulting in the gapped BdG band structure.[55] The nontrivial Berry phase carried by the nodal points and the crystallographic anisotropy of the emerged gapless Majorana modes confirm that the SC/BA_2PbCl_4/FM heterostructure realizes the exotic NSC. For $\mu < E_{CBM}$, where E_{CBM} represents the conduction band minimum at the Γ point, the condition for the NSC phase is the same as that for the TSC phase[26,56,57] and expressed by the equation $(\mu - E_{CBM})^2 + \Delta^2 < B^2$. While for $\mu \geq E_{CBM}$, one obtains NSC phase when $\Delta^2 < B^2$ (see Note 2 and Figures S4−S6 in the SI for details). With $\Delta = 0.05$ eV, the phase diagram of the NSC in the parameter space of μ and B is plotted in Figure 3e. We emphasize that although the large SOC splitting of BA_2PbCl_4 does not change the condition to get NSC, it may lead to a large nontrivial SC gap surrounding the nodal points (suppose that the *s*-wave pairing gap is large enough; therefore the induced nontrivial SC gap size is dictated by SOC-related splitting strength), which could facilitate corresponding experimental observations at a higher temperature and isolated Majorana modes in a reduced sample size (Figure S7). We also note that the realized NSC is robust against an interfacial Rashba SOC which may arise in the sandwich heterostructure (Note 3 and Figure S8 in the SI).

Ferroelectricity also plays an important role in tuning the superconducting property of materials.[58−62] Strikingly, we found that without involving complex nontrivial phase transitions of normal electronic states or ferroelectric quantum criticality, the reversal of SOC chirality alone can reverse the sign of the proximity-induced effective odd-parity pairing gap, leading to a special form of ferroelectric TSC.[49] Consequently, by modulating the polarization direction, gapless Majorana modes can emerge at the domain wall between two oppositely polarized ferroelectric domains, as we demonstrate here. Our calculations show that by switching the polarization direction of BA_2PbCl_4, the nontrivial Berry phase of the emerged nodal points changes from $\pm\pi$ to $\mp\pi$, indicating that the chirality of topological nodal points becomes opposite in two oppositely polarized domains. We then consider a nanoribbon of the SC/BA_2PbCl_4/FM heterostructure terminated along the *y*-direction, wherein the BA_2PbCl_4 monolayer consists of two oppositely polarized ferroelectric domains with the domain wall located in the middle (Figure 4a). The corresponding

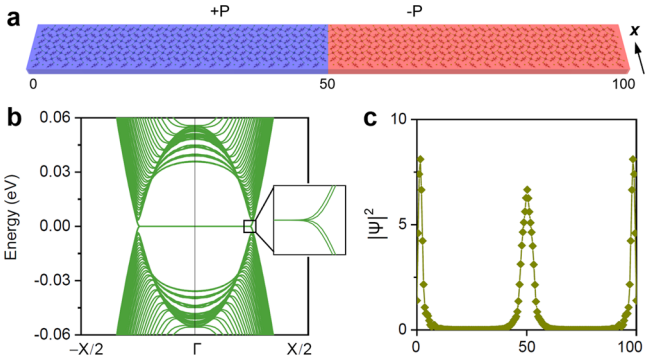

Figure 4. Domain-wall Majorana modes in the BA_2PbCl_4 monolayer. (a) Illustration of the ferroelectric two-domain structure, which is terminated along the *y*-direction and periodic along *x*-direction. The widths of the left and right domains are both 50 unit cells. (b) BdG band structure of the two-domain structure proximate to an *s*-wave SC ($\Delta = 0.05$ eV) and a FM with *y*-direction magnetization ($B = 0.1$ eV), showing the emergence of four gapless Majorana modes. (c) Real-space distributions of the four Majorana modes, peaking at the outer edges as well as the inner domain wall.

BdG band structure in Figure 4b shows the emergence of four gapless Majorana modes. By calculating the real-space distributions of the four Majorana modes, we find that they are located at the two outer edges as well as the middle domain wall, as shown in Figure 4c, indicating that the two additional gapless Majorana modes originated from the domain wall. Therefore, the intriguing gapless domain-wall Majorana modes arise.

We have demonstrated that the 2D HOIP BA_2PbCl_4 possessing large anisotropic SOC splitting and room-temperature ferroelectricity can be exploited to realize NSC and gapless Majorana edge/domain-wall modes in proximity with an *s*-wave SC and an in-plane FM. Here the monolayer is used for conceptual demonstration, but we point out that thicker films of BA_2PbCl_4, with the same point group symmetry and anisotropic SOC, are expected to harbor a similar exotic NSC phase. Some of the inorganic materials were also reported to possess similar anisotropic SOC,[63] but not in the context of ferroelectric TSC. Also, our interest in 2D HOIPs is not only piqued by this unique band structure extending the original model based on isotropic SOC[49] but also motivated by their outstanding environmental stability and inherent vdW interface providing molecularly thin films with clean surfaces. These useful features render 2D HOIPs more promising as candidates for material realization of our theoretical proposal and future device fabrication. The use of an in-plane Zeeman field also makes it possible to replace the FM with an external in-plane magnetic field that has a dominant Zeeman splitting effect and largely avoids the undesirable orbital effect.[30] The Zeeman field induced by the external magnetic field has more

https://doi.org/10.1021/acs.nanolett.3c04085
Nano Lett. 2024, 24, 2705−2711

tunability, which can be used to directly observe the topological phase transition through increasing the strength of the field, providing a diagnostic method to identify the emergence of the topological phase. It is noteworthy that Majorana modes have also been reported in proximate topological insulators combining s-wave pairing and in-plane Zeeman field.[64−66] Therein, the exploited spin-momentum-locking property is tied to the topological boundary states, while in the present work, the invoked electronic states are not necessarily topological with the spin-momentum-locking property provided by SOC, which happens to be anisotropic in 2D HOIPs.

To exploit the conduction band of 2D HOIPs and its spin-momentum-locking property, advanced doping strategies are required that do not affect its intrinsic property, indicating that strong hybridization between the semiconductor and neighboring materials[67] should be suppressed. Among various doping strategies, electrostatic gating is one promising method and has been successfully employed in previous studies of TSC in superconductor−semiconductor heterostructures[26,27,30,35,68,69] and of MoS_2 for Ising superconductivity.[70,71] In addition, given the hybrid inorganic−organic feature of 2D HOIPs, molecular doping by appropriate molecular dopants[72,73] is another promising way to achieve doping while preserving high sample quality. It is also worth noting that the controlled electronic doping itself is an important topic and has attracted increasing interest in the field of HOIPs as semiconductors,[74] and our findings would stimulate more efforts toward this direction. For experimental verification of the proposed NSC, knowledge and experience can be drawn from previous studies of Rashba-semiconductor-based TSC where the doping and SC-proximity requirements are similar to the case here.[68] Finally, the NSC is enabled by the anisotropic SOC effect (a simplified minimal model is presented in Note 4 and Figure S9 of the SI to elaborate on the same physics), which implies the possibility of realizing other novel extrinsic superconducting states by involving more complex SOC forms of the constituent semiconductors. Our findings unveil the great promise of 2D HOIPs with diverse noncentrosymmetric space groups in realizing nontrivial superconducting states and Majorana zero modes and advocate further theoretical and experimental explorations.

■ ASSOCIATED CONTENT

Supporting Information

The Supporting Information is available free of charge at https://pubs.acs.org/doi/10.1021/acs.nanolett.3c04085.

Methods for first-principles calculations and Berry phase calculations, derivation of the SOC Hamiltonian, detailed analysis of the NSC phase diagram; NSC phase in the presence of Rashba SOC, a simplified minimal model study, and additional figures as described in the text (PDF)

■ AUTHOR INFORMATION

Corresponding Author

Feng Liu − *Department of Materials Science and Engineering, University of Utah, Salt Lake City, Utah 84112, United States;* orcid.org/0000-0002-3701-8058; Email: fliu@eng.utah.edu

Authors

Xiaoyin Li − *Department of Materials Science and Engineering, University of Utah, Salt Lake City, Utah 84112, United States;* orcid.org/0000-0002-6837-7766

Shunhong Zhang − *International Center for Quantum Design of Functional Materials (ICQD), University of Science and Technology of China, Hefei, Anhui 230026, People's Republic of China;* orcid.org/0000-0003-2120-4574

Xiaoming Zhang − *College of Physics and Optoelectronic Engineering, Ocean University of China, Qingdao, Shandong 266100, People's Republic of China;* orcid.org/0000-0003-0756-9526

Zeev Valy Vardeny − *Department of Physics & Astronomy, University of Utah, Salt Lake City, Utah 84112, United States;* orcid.org/0000-0002-2298-398X

Complete contact information is available at: https://pubs.acs.org/10.1021/acs.nanolett.3c04085

Notes

The authors declare no competing financial interest.

■ ACKNOWLEDGMENTS

X.L. and F.L. acknowledge financial support from the DOE-BES (No. DE-FG02-04ER46148). X.L. acknowledges also the National Science Foundation (No. 2326228). S.Z. acknowledges financial support by the National Natural Science Foundation of China (No. 11904350) and Anhui Provincial Natural Science Foundation (2008085QA30). X.Z. acknowledges financial support by the National Natural Science Foundation of China (No. 12004357), the Natural Science Foundation of Shandong Province (No. ZR2020QA053), and the Young Talents Project at Ocean University of China. Z.V.V. acknowledges support from the DOE-BES (Grant DESC0014579). Computational resources for this work were supported by CHPC of the University of Utah and the DOE-NERSC.

■ REFERENCES

(1) Saparov, B.; Mitzi, D. B. Organic-Inorganic Perovskites: Structural Versatility for Functional Materials Design. *Chem. Rev.* **2016**, *116* (7), 4558−4596.

(2) Mao, L.; Stoumpos, C. C.; Kanatzidis, M. G. Two-Dimensional Hybrid Halide Perovskites: Principles and Promises. *J. Am. Chem. Soc.* **2019**, *141* (3), 1171−1190.

(3) Mohanty, P. P.; Ahuja, R.; Chakraborty, S. Progress and challenges in layered two-dimensional hybrid perovskites. *Nanotechnology* **2022**, *33* (29), 292501.

(4) Zhou, H.; Chen, Q.; Li, G.; Luo, S.; Song, T.-b.; Duan, H.-S.; Hong, Z.; You, J.; Liu, Y.; Yang, Y. Interface engineering of highly efficient perovskite solar cells. *Science* **2014**, *345* (6196), 542−546.

(5) Zhao, Y.; Zhu, K. Organic-inorganic hybrid lead halide perovskites for optoelectronic and electronic applications. *Chem. Soc. Rev.* **2016**, *45* (3), 655−689.

(6) Dong, Y.; Zhang, Y.; Li, X.; Feng, Y.; Zhang, H.; Xu, J. Chiral Perovskites: Promising Materials toward Next-Generation Optoelectronics. *Small* **2019**, *15* (39), 1902237.

(7) Ma, J.; Wang, H.; Li, D. Recent Progress of Chiral Perovskites: Materials, Synthesis, and Properties. *Adv. Mater.* **2021**, *33* (26), 2008785.

(8) Zheng, W.; Wang, X.; Zhang, X.; Chen, B.; Suo, H.; Xing, Z.; Wang, Y.; Wei, H.-L.; Chen, J.; Guo, Y.; Wang, F. Emerging Halide Perovskite Ferroelectrics. *Adv. Mater.* **2023**, *35* (21), 2205410.

(9) Chakraborty, R.; Rajput, P. K.; Anilkumar, G. M.; Maqbool, S.; Das, R.; Rahman, A.; Mandal, P.; Nag, A. Rational Design of Non-

Centrosymmetric Hybrid Halide Perovskites. *J. Am. Chem. Soc.* **2023**, *145* (2), 1378−1388.
(10) Lu, H.; Vardeny, Z. V.; Beard, M. C. Control of light, spin and charge with chiral metal halide semiconductors. *Nat. Rev. Chem.* **2022**, *6* (7), 470−485.
(11) Kim, Y.-H.; Zhai, Y.; Lu, H.; Pan, X.; Xiao, C.; Gaulding, E. A.; Harvey, S. P.; Berry, J. J.; Vardeny, Z. V.; Luther, J. M.; Beard, M. C. Chiral-induced spin selectivity enables a room-temperature spin light-emitting diode. *Science* **2021**, *371* (6534), 1129−1133.
(12) Kepenekian, M.; Robles, R.; Katan, C.; Sapori, D.; Pedesseau, L.; Even, J. Rashba and Dresselhaus Effects in Hybrid Organic-Inorganic Perovskites: From Basics to Devices. *ACS Nano* **2015**, *9* (12), 11557−11567.
(13) Jia, F.; Hu, S.; Xu, S.; Gao, H.; Zhao, G.; Barone, P.; Stroppa, A.; Ren, W. Persistent Spin-texture and Ferroelectric Polarization in 2D Hybrid Perovskite Benzylammonium Lead-halide. *J. Phys. Chem. Lett.* **2020**, *11* (13), 5177−5183.
(14) Zhang, L.; Jiang, J.; Multunas, C.; Ming, C.; Chen, Z.; Hu, Y.; Lu, Z.; Pendse, S.; Jia, R.; Chandra, M.; Sun, Y.-Y.; Lu, T.-M.; Ping, Y.; Sundararaman, R.; Shi, J. Room-temperature electrically switchable spin-valley coupling in a van der Waals ferroelectric halide perovskite with persistent spin helix. *Nat. Photonics* **2022**, *16* (7), 529−537.
(15) Guo, W.; Xu, H.; Ma, Y.; Liu, Y.; Gao, H.; Hu, T.; Ren, W.; Luo, J.; Sun, Z. Electrically Switchable Persistent Spin Texture in a Two-Dimensional Hybrid Perovskite Ferroelectric. *Angew. Chem., Int. Ed.* **2023**, *62* (17), No. e202300028.
(16) Leng, K.; Li, R.; Lau, S. P.; Loh, K. P. Ferroelectricity and Rashba effect in 2D organic-inorganic hybrid perovskites. *Trends Chem.* **2021**, *3* (9), 716−732.
(17) Ricciardulli, A. G.; Yang, S.; Smet, J. H.; Saliba, M. Emerging perovskite monolayers. *Nat. Mater.* **2021**, *20* (10), 1325−1336.
(18) Li, C.; Loh, K. P.; Leng, K. Organic-inorganic hybrid perovskites and their heterostructures. *Matter* **2022**, *5* (12), 4153−4169.
(19) Volovik, G. E. Fermion zero modes on vortices in chiral superconductors. *JETP Lett.* **1999**, *70* (9), 609−614.
(20) Read, N.; Green, D. Paired states of fermions in two dimensions with breaking of parity and time-reversal symmetries and the fractional quantum Hall effect. *Phys. Rev. B* **2000**, *61* (15), 10267−10297.
(21) Ivanov, D. A. Non-Abelian Statistics of Half-Quantum Vortices in p-Wave Superconductors. *Phys. Rev. Lett.* **2001**, *86* (2), 268−271.
(22) Nayak, C.; Simon, S. H.; Stern, A.; Freedman, M.; Das Sarma, S. Non-Abelian anyons and topological quantum computation. *Rev. Mod. Phys.* **2008**, *80* (3), 1083−1159.
(23) Qi, X.-L.; Zhang, S.-C. Topological insulators and superconductors. *Rev. Mod. Phys.* **2011**, *83* (4), 1057−1110.
(24) Fu, L.; Kane, C. L. Superconducting Proximity Effect and Majorana Fermions at the Surface of a Topological Insulator. *Phys. Rev. Lett.* **2008**, *100* (9), 096407.
(25) Sato, M.; Ando, Y. Topological superconductors: a review. *Rep. Prog. Phys.* **2017**, *80* (7), 076501.
(26) Sau, J. D.; Lutchyn, R. M.; Tewari, S.; Das Sarma, S. Generic New Platform for Topological Quantum Computation Using Semiconductor Heterostructures. *Phys. Rev. Lett.* **2010**, *104* (4), 040502.
(27) Lutchyn, R. M.; Sau, J. D.; Das Sarma, S. Majorana Fermions and a Topological Phase Transition in Semiconductor-Superconductor Heterostructures. *Phys. Rev. Lett.* **2010**, *105* (7), 077001.
(28) Oreg, Y.; Refael, G.; von Oppen, F. Helical Liquids and Majorana Bound States in Quantum Wires. *Phys. Rev. Lett.* **2010**, *105* (17), 177002.
(29) Kitaev, A. Y. Unpaired Majorana fermions in quantum wires. *Physics-Uspekhi* **2001**, *44* (10S), 131.
(30) Alicea, J. Majorana fermions in a tunable semiconductor device. *Phys. Rev. B* **2010**, *81* (12), 125318.
(31) Zhang, X.; Liu, J.; Liu, F. Topological Superconductivity Based on Antisymmetric Spin-Orbit Coupling. *Nano Lett.* **2022**, *22* (22), 9000−9005.
(32) Zhang, H.; Liu, C.-X.; Gazibegovic, S.; Xu, D.; Logan, J. A.; Wang, G.; van Loo, N.; Bommer, J. D. S.; de Moor, M. W. A.; Car, D.; Op het Veld, R. L. M.; van Veldhoven, P. J.; Koelling, S.; Verheijen, M. A.; Pendharkar, M.; Pennachio, D. J.; Shojaei, B.; Lee, J. S.; Palmstrøm, C. J.; Bakkers, E. P. A. M.; Sarma, S. D.; Kouwenhoven, L. P. RETRACTED ARTICLE: Quantized Majorana conductance. *Nature* **2018**, *556* (7699), 74−79.
(33) Lutchyn, R. M.; Bakkers, E. P. A. M.; Kouwenhoven, L. P.; Krogstrup, P.; Marcus, C. M.; Oreg, Y. Majorana zero modes in superconductor-semiconductor heterostructures. *Nat. Rev. Mater.* **2018**, *3* (5), 52−68.
(34) Frolov, S. M.; Manfra, M. J.; Sau, J. D. Topological superconductivity in hybrid devices. *Nat. Phys.* **2020**, *16* (7), 718−724.
(35) Prada, E.; San-Jose, P.; de Moor, M. W. A.; Geresdi, A.; Lee, E. J. H.; Klinovaja, J.; Loss, D.; Nygård, J.; Aguado, R.; Kouwenhoven, L. P. From Andreev to Majorana bound states in hybrid superconductor-semiconductor nanowires. *Nat. Rev. Phys.* **2020**, *2* (10), 575−594.
(36) Braun, M.; Frey, W. Crystal structure of bis(benzylammonium) lead tetrachloride, $(C_7H_7NH_3)_2PbCl_4$. *Z. Kristallogr. New Cryst. Struct.* **1999**, *214* (3), 331−332.
(37) Liao, W.-Q.; Zhang, Y.; Hu, C.-L.; Mao, J.-G.; Ye, H.-Y.; Li, P.-F.; Huang, S. D.; Xiong, R.-G. A lead-halide perovskite molecular ferroelectric semiconductor. *Nat. Commun.* **2015**, *6* (1), 7338.
(38) You, L.; Liu, F.; Li, H.; Hu, Y.; Zhou, S.; Chang, L.; Zhou, Y.; Fu, Q.; Yuan, G.; Dong, S.; Fan, H. J.; Gruverman, A.; Liu, Z.; Wang, J. In-Plane Ferroelectricity in Thin Flakes of Van der Waals Hybrid Perovskite. *Adv. Mater.* **2018**, *30* (51), 1803249.
(39) Yang, Y.; Lou, F.; Xiang, H. Cooperative Nature of Ferroelectricity in Two-Dimensional Hybrid Organic-Inorganic Perovskites. *Nano Lett.* **2021**, *21* (7), 3170−3176.
(40) Sato, M.; Fujimoto, S. Existence of Majorana Fermions and Topological Order in Nodal Superconductors with Spin-Orbit Interactions in External Magnetic Fields. *Phys. Rev. Lett.* **2010**, *105* (21), 217001.
(41) Sato, M.; Tanaka, Y.; Yada, K.; Yokoyama, T. Topology of Andreev bound states with flat dispersion. *Phys. Rev. B* **2011**, *83* (22), 224511.
(42) Li, Y.; Haldane, F. D. M. Topological Nodal Cooper Pairing in Doped Weyl Metals. *Phys. Rev. Lett.* **2018**, *120* (6), 067003.
(43) Huang, B.; Yang, X.; Xu, N.; Gong, M. Type-I and type-II topological nodal superconductors with s-wave interaction. *Phys. Rev. B* **2018**, *97* (4), 045142.
(44) Zhang, R.-X.; Cole, W. S.; Wu, X.; Das Sarma, S. Higher-Order Topology and Nodal Topological Superconductivity in Fe(Se,Te) Heterostructures. *Phys. Rev. Lett.* **2019**, *123* (16), 167001.
(45) Bazarnik, M.; Lo Conte, R.; Mascot, E.; von Bergmann, K.; Morr, D. K.; Wiesendanger, R. Antiferromagnetism-driven two-dimensional topological nodal-point superconductivity. *Nat. Commun.* **2023**, *14* (1), 614.
(46) He, W.-Y.; Zhou, B. T.; He, J. J.; Yuan, N. F. Q.; Zhang, T.; Law, K. T. Magnetic field driven nodal topological superconductivity in monolayer transition metal dichalcogenides. *Commun. Phys.* **2018**, *1* (1), 40.
(47) Margalit, G.; Berg, E.; Oreg, Y. Theory of multi-orbital topological superconductivity in transition metal dichalcogenides. *Ann. Phys.* **2021**, *435*, 168561.
(48) Nayak, A. K.; Steinbok, A.; Roet, Y.; Koo, J.; Margalit, G.; Feldman, I.; Almoalem, A.; Kanigel, A.; Fiete, G. A.; Yan, B.; Oreg, Y.; Avraham, N.; Beidenkopf, H. Evidence of topological boundary modes with topological nodal-point superconductivity. *Nat. Phys.* **2021**, *17* (12), 1413−1419.
(49) Zhang, X.; Zhao, P.; Liu, F. Ferroelectric topological superconductor. *arXiv (cond-mat.mtrl-sci)* 2024, arXiv:2401.05847, https://arxiv.org/abs/2401.05847 (accessed January 11, 2024).
(50) Rashba, E. Properties of semiconductors with an extremum loop. I. Cyclotron and combinational resonance in a magnetic field perpendicular to the plane of the loop. *Sov. Phys. Solid State* **1960**, *2*, 1109.

https://doi.org/10.1021/acs.nanolett.3c04085
Nano Lett. 2024, 24, 2705−2711

(51) Wang, L.; Yao, X.; Sun, Y.; Wu, W.; He, A.; Liu, Y.; Zhang, X. Robust ferromagnetism and Weyl half-semimetal in a two-dimensional vanadium boride monolayer. *Nanoscale* **2022**, *14* (34), 12491−12497.
(52) Lopes, E. V. C.; Baierle, R. J.; Miwa, R. H.; Schmidt, T. M. Noncentrosymmetric two-dimensional Weyl semimetals in porous Si/Ge structures. *arXiv (cond-mat.mtrl-sci)* 2023, arXiv:2305.05756, https://arxiv.org/abs/2305.05756 (accessed May 9, 2023).
(53) Wang, Z. F.; Chen, L.; Liu, F. Tuning Topological Edge States of Bi(111) Bilayer Film by Edge Adsorption. *Nano Lett.* **2014**, *14* (5), 2879−2883.
(54) Wang, Z. F.; Zhang, H.; Liu, D.; Liu, C.; Tang, C.; Song, C.; Zhong, Y.; Peng, J.; Li, F.; Nie, C.; Wang, L.; Zhou, X. J.; Ma, X.; Xue, Q. K.; Liu, F. Topological edge states in a high-temperature superconductor FeSe/SrTiO3(001) film. *Nat. Mater.* **2016**, *15* (9), 968−973.
(55) Zhang, X.; Gao, D.; Zhu, X.; Liu, J.; Wang, W.; Liu, X.; Zhao, M. Prediction of topological superconductivity from type-IV, -III, -II, and -I' nodal points induced by Rashba spin-orbit coupling. *Phys. Rev. B* **2021**, *104* (24), 245409.
(56) Sato, M.; Takahashi, Y.; Fujimoto, S. Non-Abelian Topological Order in s-Wave Superfluids of Ultracold Fermionic Atoms. *Phys. Rev. Lett.* **2009**, *103* (2), 020401.
(57) Yamakage, A.; Tanaka, Y.; Nagaosa, N. Evolution of Edge States and Critical Phenomena in the Rashba Superconductor with Magnetization. *Phys. Rev. Lett.* **2012**, *108* (8), 087003.
(58) Rowley, S. E.; Spalek, L. J.; Smith, R. P.; Dean, M. P. M.; Itoh, M.; Scott, J. F.; Lonzarich, G. G.; Saxena, S. S. Ferroelectric quantum criticality. *Nat. Phys.* **2014**, *10* (5), 367−372.
(59) Edge, J. M.; Kedem, Y.; Aschauer, U.; Spaldin, N. A.; Balatsky, A. V. Quantum Critical Origin of the Superconducting Dome in $SrTiO_3$. *Phys. Rev. Lett.* **2015**, *115* (24), 247002.
(60) Kozii, V.; Klein, A.; Fernandes, R. M.; Ruhman, J. Synergetic Ferroelectricity and Superconductivity in Zero-Density Dirac Semimetals near Quantum Criticality. *Phys. Rev. Lett.* **2022**, *129* (23), 237001.
(61) Chen, J.; Qin, W.; Cui, P.; Zhang, Z. Ferroelectric tuning of superconductivity and band topology in a two-dimensional heterobilayer. *Phys. Rev. B* **2023**, *108* (6), L060501.
(62) Chen, J.; Qin, W.; Cui, P.; Zhang, Z. Enhanced stability and superconductivity of $IrTe_2/In_2Se_3$ heterobilayers with ferroelectrically switchable band topology. *Phys. Rev. B* **2023**, *108* (8), 085408.
(63) Tao, L. L.; Tsymbal, E. Y. Persistent spin texture enforced by symmetry. *Nat. Commun.* **2018**, *9* (1), 2763.
(64) Pan, X.-H.; Yang, K.-J.; Chen, L.; Xu, G.; Liu, C.-X.; Liu, X. Lattice-Symmetry-Assisted Second-Order Topological Superconductors and Majorana Patterns. *Phys. Rev. Lett.* **2019**, *123* (15), 156801.
(65) Wu, Y.-J.; Hou, J.; Li, Y.-M.; Luo, X.-W.; Shi, X.; Zhang, C. In-Plane Zeeman-Field-Induced Majorana Corner and Hinge Modes in an s-Wave Superconductor Heterostructure. *Phys. Rev. Lett.* **2020**, *124* (22), 227001.
(66) Wang, C.; Liu, F.; Huang, H. Effective Model for Fractional Topological Corner Modes in Quasicrystals. *Phys. Rev. Lett.* **2022**, *129* (5), 056403.
(67) Trainer, D. J.; Wang, B.; Bobba, F.; Samuelson, N.; Xi, X.; Zasadzinski, J.; Nieminen, J.; Bansil, A.; Iavarone, M. Proximity-Induced Superconductivity in Monolayer MoS2. *ACS Nano* **2020**, *14* (3), 2718−2728.
(68) Mourik, V.; Zuo, K.; Frolov, S. M.; Plissard, S. R.; Bakkers, E. P. A. M.; Kouwenhoven, L. P. Signatures of Majorana Fermions in Hybrid Superconductor-Semiconductor Nanowire Devices. *Science* **2012**, *336* (6084), 1003−1007.
(69) Gül, Ö.; Zhang, H.; Bommer, J. D. S.; de Moor, M. W. A.; Car, D.; Plissard, S. R.; Bakkers, E. P. A. M.; Geresdi, A.; Watanabe, K.; Taniguchi, T.; Kouwenhoven, L. P. Ballistic Majorana nanowire devices. *Nat. Nanotechnol.* **2018**, *13* (3), 192−197.
(70) Lu, J. M.; Zheliuk, O.; Leermakers, I.; Yuan, N. F. Q.; Zeitler, U.; Law, K. T.; Ye, J. T. Evidence for two-dimensional Ising superconductivity in gated MoS2. *Science* **2015**, *350* (6266), 1353−1357.
(71) Saito, Y.; Nakamura, Y.; Bahramy, M. S.; Kohama, Y.; Ye, J.; Kasahara, Y.; Nakagawa, Y.; Onga, M.; Tokunaga, M.; Nojima, T.; Yanase, Y.; Iwasa, Y. Superconductivity protected by spin-valley locking in ion-gated MoS2. *Nat. Phys.* **2016**, *12* (2), 144−149.
(72) Kambe, T.; Sakamoto, R.; Kusamoto, T.; Pal, T.; Fukui, N.; Hoshiko, K.; Shimojima, T.; Wang, Z.; Hirahara, T.; Ishizaka, K.; Hasegawa, S.; Liu, F.; Nishihara, H. Redox Control and High Conductivity of Nickel Bis(dithiolene) Complex π-Nanosheet: A Potential Organic Two-Dimensional Topological Insulator. *J. Am. Chem. Soc.* **2014**, *136* (41), 14357−14360.
(73) Sun, X.; Wu, K.-H.; Sakamoto, R.; Kusamoto, T.; Maeda, H.; Ni, X.; Jiang, W.; Liu, F.; Sasaki, S.; Masunaga, H.; Nishihara, H. Bis(aminothiolato)nickel nanosheet as a redox switch for conductivity and an electrocatalyst for the hydrogen evolution reaction. *Chem. Sci.* **2017**, *8* (12), 8078−8085.
(74) Amerling, E.; Lu, H.; Larson, B. W.; Maughan, A. E.; Phillips, A.; Lafalce, E.; Whittaker-Brooks, L.; Berry, J. J.; Beard, M. C.; Vardeny, Z. V.; Blackburn, J. L. A Multi-Dimensional Perspective on Electronic Doping in Metal Halide Perovskites. *ACS Energy Lett.* **2021**, *6* (3), 1104−1123.

https://doi.org/10.1021/acs.nanolett.3c04085
Nano Lett. 2024, 24, 2705−2711